Exosomes derived from human umbilical cord mesenchymal stem cells alleviate Parkinson's disease and neuronal damage through inhibition of microglia

Zhong-Xia Zhang[1, #], Yong-Jie Zhou[2, #], Ping Gu[1], Wei Zhao[2], Hong-Xu Chen[2], Ruo-Yu Wu[2], Lu-Yang Zhou[2], Qing-Zhuo Cui[2], Shao-Kang Sun[2], Lin-Qi Zhang[2], Ke Zhang[2], Hong-Jun Xu[2], Xi-Qing Chai[1, *], Sheng-Jun An[2, *]

https://doi.org/10.4103/1673-5374.368300

Date of submission: September 4, 2022

Date of decision: November 19, 2022

Date of acceptance: December 6, 2022

Date of web publication: January 30, 2023

From the Contents

Graphical Abstract

Human umbilical cord mesenchymal stem cell-derived exosomes may play a crucial role in protecting dopamine neurons by inhibiting microglia in vivo and in vitro

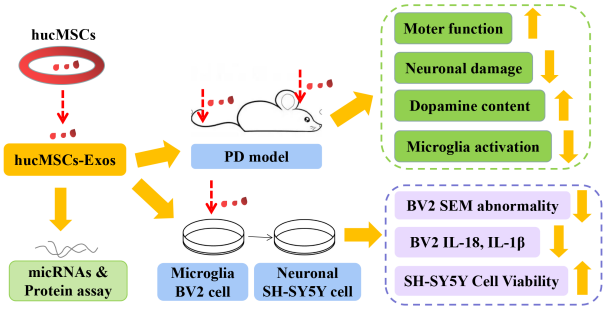

Abstract

Microglia-mediated inflammatory responses have been shown to play a crucial role in Parkinson's disease. In addition, exosomes derived from mesenchymal stem cells have shown anti-inflammatory effects in the treatment of a variety of diseases. However, whether they can protect neurons in Parkinson's disease by inhibiting microglia-mediated inflammatory responses is not yet known. In this study, exosomes were isolated from human umbilical cord mesenchymal stem cells and injected into a 6-hydroxydopamine-induced rat model of Parkinson's disease. We found that the exosomes injected through the tail vein and lateral ventricle were absorbed by dopaminergic neurons and microglia on the affected side of the brain, where they repaired nigral-striatal dopamine system damage and inhibited microglial activation. Furthermore, in an *in vitro* cell model, pretreating lipopolysaccharide-stimulated BV2 cells with exosomes reduced interleukin-1β and interleukin-18 secretion, prevented the adoption of pyroptosis-associated morphology by BV2 cells, and increased the survival rate of SH-SY5Y cells. Potential targets for treatment with human umbilical cord mesenchymal stem cells and exosomes were further identified by high-throughput microRNA sequencing and protein spectrum sequencing. Our findings suggest that human umbilical cord mesenchymal stem cells and exosomes are a potential treatment for Parkinson's disease, and that their neuroprotective effects may be mediated by inhibition of excessive microglial proliferation.

Key Words: 6-hydroxydopamine; dopamine neurons; exosomes; inflammation; mesenchymal stem cells; microglia; Parkinson's disease; pyroptosis

Introduction

Parkinson's disease (PD) is the second most common neurodegenerative disease, and its main clinical manifestations are static tremor, bradykinesia, myotonia, and abnormalities of posture and gait. The main pathological changes are degenerative death of dopaminergic neurons in the substantia nigra (SN) and a decrease in dopamine (DA) content in the striatum. Microglia, as the primary resident immune cells of the central nervous system (CNS), originate from yolk-sac myeloid cells that migrate during the embryonic development to populate the CNS parenchyma (Ransohoff and Cardona, 2010). Since McGeer et al. (1988) first observed microglial activation in the SN and basal ganglia in autopsy specimens from PD patients in the 1980s, many additional autopsy, brain imaging, and fluid biomarker studies have suggested that microglia-mediated neuroinflammation plays an important role in the pathogenesis and progression of PD (Croisier et al., 2005; Ouchi et al., 2005; Brochard et al., 2009). This is strongly supported by the involvement of the microglial NOD-like receptor family pyrin domain containing 3 (NLRP3) inflammasome (Gordon et al., 2018; Adams, et al., 2019; Ahmed et al., 2021), which is an important component of the immune system that mediates pyroptosis. Pyroptosis is a newly described form of programmed cell death that is mediated by the pore-forming effects of the gasdermin protein family, a mechanism that is distinct from those involved in apoptosis and autophagy (Shi et al., 2017; Bertheloot et al., 2021). Studies that included clinical data and experiments performed in PD animal models showed that microglia-mediated pyroptosis plays a key role in PD (Stefanova, 2022).

Human umbilical cord mesenchymal stem cells (hucMSCs), which are plentiful, easy to harvest, and have low immunogenicity, improve the behavioral performance of PD animal models and the clinical symptoms of PD patients (Weiss et al., 2006; Chung et al., 2018). However, they are limited in that their activity does not last long, they are difficult to quantify, and they do not penetrate the blood-brain barrier. Exosomes (Exos), a type of extracellular vesicles, are lipid bi-layer membrane vesicles with a diameter of 30–150 nm that are actively released by most cells. Various bioactive molecules, including proteins, lipids, and nucleic acids, are enriched in Exos. Exos shuttle these molecular cargoes from donor cells to recipient cells and play an important role in mediating intercellular communication (Zhang et al., 2015; Yu et al., 2022). Accumulating evidence suggests that Exos derived from MSCs elicit similar therapeutic effects to their parent MSCs (Zhang et al., 2022); furthermore, they have striking advantages over whole-cell therapy such as

[1]Department of Neurology, the First Affiliated Hospital of Hebei Medical University, Shijiazhuang, Hebei Province, China; [2]Research Center, Hebei University of Chinese Medicine, Shijiazhuang, Hebei Province, China

*Correspondence to: Xi-Qing Chai, MD, hbykdxzzx@126.com; Sheng-Jun An, MD, PhD, sjsjan@126.com.

https://orcid.org/0000-0002-2643-3459 (Xi-Qing Chai); https://orcid.org/0000-0001-8765-0396 (Sheng-Jun An)

#Both authors contributed equally to this work.

Funding: *This work was supported by the Natural Science Foundation of Hebei Province, Nos. 18967728D (to XQC), H2021423063 (to HXC); Youth Top Talent Project of Colleges and Universities in Hebei Province, No. BJ2021033 (to HXC).*

How to cite this article: *Zhang ZX, Zhou YJ, Gu P, Zhao W, Chen HX, Wu RY, Zhou LY, Cui QZ, Sun SK, Zhang LQ, Zhang K, Xu HJ, Chai XQ, An SJ (2023) Exosomes derived from human umbilical cord mesenchymal stem cells alleviate Parkinson's disease and neuronal damage through inhibition of microglia. Neural Regen Res 18(10):2291-2300.*

low immunogenicity and high biosafety. Several studies have shown that Exos secreted by MSCs have great promise in the treatment of certain diseases, such as cancer and stroke, as well as in wound-healing. Human umbilical cord mesenchymal stem cell-derived exosomes (hucMSC-Exos) have been shown to reduce liver damage (Zhang et al., 2020), retinitis (Zhang et al., 2019), and ischemic damage (Yan et al., 2015) through inhibiting inflammation or pyroptosis. However, it remains unknown whether hucMSC-Exos improve PD by inhibiting microglia-mediated pyroptosis.

We previously reported that hucMSCs-Exos induce neuronal autophagy in a PD rat model (Chen et al., 2020). Therefore, the aim of this study was to investigate whether the neuroprotective effect of hucMSC-Exos on PD in the rat model is related to inhibition of microglial activation *in vivo* and inhibition of microglia-mediated pyroptosis *in vitro*. Moreover, we carried out a preliminary investigation of the possible underlying mechanism using miRNA sequencing, protein spectrum sequencing, and bioinformatics analysis.

Methods

Cell culture

Fresh umbilical cords for which there were no ethical disputes were obtained from normal spontaneous full-term deliveries by mothers at the Obstetrics Department of the First Hospital of Hebei Medical University who provided informed consent. The umbilical cord samples were stored in sterile phosphate-buffered saline (PBS), transported to the laboratory at Hebei University of Chinese Medicine, and processed within 3–6 hours. The outer membrane, arteries, and veins were removed from the sterile umbilical cords under aseptic conditions. Then, the Watson's jelly was obtained, cut into 1-cm^2 pieces, and cultured in serum-free mesenchymal stem cell complete medium (Yocon, Beijing, China; Cat# NCO103) at 37°C in a 5% CO_2 incubator (Thermo Fisher Scientific, Waltham, MA, USA). HucMSCs on passage three were used in the following experiments. The human neuroblastoma cell line SH-SY5Y (China Center for Type Culture Collection, Wuhan, China, Cat# GDC0210) and the mouse microglial cell line BV2 (Cat# STCC20009G; Servicebio, Wuhan, China) were cultured in DMEM/F12 containing 10% fetal bovine serum (Thermo Fisher Scientific) at 37°C in a 5% CO_2 incubator. All experiments were approved by the Ethics Committee of the First Affiliated Hospital of Hebei Medical University on June 5, 2018 (approval No. 2018040319).

Cell morphology was observed by optical microscope (Olympus, Tokyo, Japan). Cells were seeded into 12-well culture plates, and cell counts were performed for three wells at the same time every day for 7 consecutive days starting on the second day of culturing. To do this, the cells were stained with trypan blue (Sigma, St. Louis, MO, USA) and manually counted, a growth curve was drawn, and cell proliferation was calculated.

HucMSC identification

HucMSC surface marker proteins were assayed by flow cytometry (Beckman Coulter, Pasadena, CA, USA). HucMSCs were digested, centrifuged, and suspended in PBS. Then, fluorescein isothiocyanate (FITC)-conjugated antibodies to CD73 (mouse; BD Biosciences, Sparks, MD, USA, Cat# 561254, RRID: AB_10894209), CD90 (mouse; BD Biosciences, Cat# 555595, RRID: AB_395969), CD34 (mouse; BD Biosciences, Cat# 560238, RRID: AB_1645242), and HLA-DR (mouse; BD Biosciences, Cat# 555811, RRID: AB_396145), and phycoerythrin (PE)-conjugated antibodies to CD 105 (mouse; BD Biosciences, Cat# 560839, RRID: AB_2033932) and CD45 (mouse; BD Biosciences, Cat# 555483, RRID: AB_395875) were added, and the cells were incubated on ice for 15–20 minutes then assayed.

The multidirectional differentiation potential of hucMSCs was evaluated. A three-line inductive differentiation medium kit containing adipogenic, osteogenic, and chondrogenic differentiation medium (Biological Industries, Beit-Haemek, Israel) was used, and the cells were monitored for 3–4 weeks. Oil red O staining (Biological Industries) was used to stain the lipid droplets, alizarin red (Biological Industries) was used to stain the calcium nodules, and Alcian blue (Biological Industries) was used to stain the acid mucopolysaccharide in the cartilage tissue. Adipogenic, osteogenic, and chondrogenic differentiation were observed by optical microscope.

HucMSC-Exo purification

Spent hucMSCs culture medium was collected, and ultra-high speed differential centrifugation (Sorvall™WX+, Thermo Scientific™, USA) was used to extract Exos as described previously (Chen, et al., 2020). Briefly, the medium was centrifuged at 2000 × *g* at 4°C for 20 minutes, and the resulting supernatant was centrifuged at 10,000 × *g* at 4°C for 30 minutes and then again at 10,000 × *g* at 4°C for 70 minutes. The resulting pellet contained the isolated Exos.

Evaluation of hucMSC-Exos by transmission electron microscopy

For the identification of hucMSC-Exos (Witwer et al., 2017), the cell morphology was examined by transmission electron microscopy (TEM). HucMSC-Exos were negatively stained with 2% uranyl acetate (Sigma) and dried at 120 kV for 10 minutes. Then, the morphology was observed by TEM (H-7650, Hitachi, Tokyo, Japan).

Identification of hucMSC-Exos by nanoparticle tracking analysis

The size distribution of hucMSC-Exos was evaluated by Nanoparticle Tracking Analysis (NTA). PBS was used to dilute Exos to 1×10^7–1×10^9 particles/mL, and nanoparticle potentiometric titration using a particle size analyzer (ZetaView PMX 110, Particle Metri, Meerbusch, Germany) set to an emission wavelength of 405 nm was used to determine particle size and quantity.

Western blot analysis

Western blotting was used to assay for the presence of surface specific proteins on hucMSC-Exos, and the concentrations were determined using a BCA Protein Assay Kit (Solarbio, Beijing, China). An equal amount of protein for each sample (20–30 μg) was subjected to electrophoresis and transferred to a polyvinylidene difluoride membrane (Millipore, Burlington, MA, USA). The membrane was then sealed in a plastic pouch containing 5% skimmed milk and incubated at 37°C for 1 hour. The protein samples were incubated with the following primary antibodies overnight at 4°C: TSG101 (mouse, 1:500; Cat# sc-13611, Santa Cruz Biotechnology, Santa Cruz, CA, USA), CD63 (mouse, 1:1000; Cat# sc-5275(M), Santa Cruz Biotechnology), Alix (mouse, 1:1000; Santa Cruz Biotechnology, Cat# sc-53540, RRID: AB_673819), Calnexin (rabbit, 1:1000; Proteintech, Rosemont, IL, USA, Cat# 10427-2-AP, RRID: AB_2069033). After washing with Tris-buffered saline containing Tween 20 (TBST), the membranes were incubated with secondary antibodies (goat anti-mouse IgG H&L (HRP), 1:10,000; Abcam, Cambridge, UK, Cat# ab6789, RRID: AB_955439; goat anti-rabbit IgG H&L (HRP), 1:10000; Abcam, Cat# ab6721, RRID: AB_955447) at 37°C for 1 hour. Finally, the proteins were detected with ECL developer (Millipore), and photographed using a GS 800 Densitometer Scanner (GMI, Ramsey, MN, USA).

Animals

SPF closed-colony male Sprague-Dawley Rats weighing 200–220 g (Hebei Invivo Biotechnology Co., Ltd., license No. SCXK (Ji) 2019-003) were raised in a specific pathogen-free environment. Considering the relationship between PD and estrogen (Cerri et al., 2019; Avram et al., 2021), to avoid potential confounding factors that could arise from using male and female rats, and for consistency with the published literature (Chen et al., 2020; Zhang et al., 2021), only male rats were used in this study. The room temperature was 22 ± 2°C, the humidity was 45–50%, and the light/dark cycle was 12/12 hours. All the animal experiments were conducted according to the recommendations in the Guide for the Care and Use of Laboratory Animals of the National Institutes of Health, and the study was approved by the Ethics Committee of the First Affiliated Hospital of Hebei Medical University (approval No. 2018040319) on June 5, 2018.

Rats were randomly allocated to Control (non-diseased, normal) and PD model groups. Based on the APO test, rats in which PD was successfully established were randomly divided into the following groups: 6-OHDA (untreated PD), Exos-T (with Exo injection via the tail vein), and Exos-LV (with Exo injection into the lateral ventricle). The random number method was used for grouping.

Establishment of PD animal model and grouping

As described previously (Gu et al., 2012), the rat model of PD was established using a rat brain stereotactic instrument (Neurostar, Tubingen, Germany). Rats were injected with 4% isoflurane for anesthesia induction and 2% isoflurane for anesthesia maintenance and placed on the stereotactic instrument (Neurostar). A micromotor handpiece was used to create two 1-mm burr holes at coordinates corresponding to the right substantia nigra compacta (SNc) (4.4 mm posterior to the bregma, 1.2 mm right of the sagittal suture, subdural 7.8 mm) and the ventral tegmental area (VTA) (4.8 mm posterior to the bregma, 1.0 mm right of the sagittal suture, subdural 7.8 mm). The coordinates were confirmed with a stereotaxic atlas of the rat brain (Paxinos and Watson, 2006). Freshly prepared 6-OHDA (2 μL of a 4-μg/μL solution, diluted in sterile normal saline containing 0.2% ascorbic acid, Sigma) was injected into each point with a 5-μL Hamilton syringe and an infusion pump set to a rate of 0.2 μL/min. The syringe was held in place for 10 minutes after injection, then gently retracted. The control group was subjected to the same procedure and injected with the same amount (2 μL at each point) of normal saline containing 0.2% ascorbic acid. The 6-OHDA and saline solutions were filter-sterilized under sterile conditions before injection. On day 21 after surgery, apomorphine (APO, 0.5 mg/kg, Sigma) was injected intraperitoneally. Rats with an average speed in rotational number per minute greater than 7 rotations/minute were regarded as successful exemplars of the PD model.

HucMSC-Exo injection

Rats in the Exos-T group were injected with 1 mL saline containing 100 μg Exos once a day for 14 consecutive days via the tail vein. Rats in the Exos-LV group were injected with 10 μL normal saline containing 100 μg Exos in the right lateral ventricle (1.5 mm posterior to the bregma, 1.5 mm right of the sagittal suture, subdural 3.8 mm) using the rat brain stereotactic instrument according to the procedure described above, except for using a different injection point. The control and 6-OHDA groups did not receive any further intervention. Eight weeks later, all rats were anesthetized with 4% isoflurane (RWD, Shenzhen, China) and sacrificed, and the brains were harvested. The Exo dose was selected and the experimental protocol was designed based on our pretest results and previous reports (Gu et al., 2012; Shiue et al., 2019; Chen et al., 2020).

Behavioral tests

The APO induction test was performed to evaluate motor function in the rats. On the 1st day of the weeks 2, 4, 6, and 8 after hucMSC-Exo injection, APO (at the dose mentioned above) was intraperitoneally injected into the rats to induce rotation, and the number of rotations per minute was observed and recorded.

Tracking of PKH26-labeled hucMSC-Exos in the substantia nigra of the PD rat model

HucMSC-Exos were stained according to the PKH26 kit (Sigma, St. Louis, MO, USA) instructions. Briefly, Exos were incubated with 1 mL Diluent C and 4 μL PKH26 dye for 5 minutes, and then 2 mL FBS was added to block the staining reaction. The solution was centrifuged at 4 °C and 120,000 × *g* for 100 minutes to obtain a pellet containing the labeled Exos.

To verify whether hucMSC-Exos can cross the blood-brain barrier (BBB) and reach the SN, colocalization of Exos with dopaminergic neurons and microglia was observed. The rats groups and hucMSC-Exo injections were as described above. It should be noted that rats in both the Exos-T and Exos-LV groups were injected with Exos via the tail vein or lateral ventricle once. At 24 hours post-surgery, rats were deeply anesthetized and sacrificed, and the brains were harvested and transferred to 15% and 30% sucrose solution at 4°C, embedded in optimal cutting temperature (OCT) compound, and frozen. The frozen, embedded brain tissues were then sectioned at a thickness of 8 μm using a cryostat (Thermo Fisher Scientific), and the frozen sections were prepared for immunofluorescence staining.

High-performance liquid chromatography-mass spectrometry (HPLC-MS)

DA, 5-hydroxytryptamine (5-HT), and their metabolites were detected in the striatum of the rats in each group using an Ultimate 3000 RS chromatograph (Thermo Fisher Scientific) and a Q Exactive high-resolution mass spectrometer (Thermo Fisher Scientific). The electrospray voltage of the mass spectrometry ion source was 3.2 kV, the positive and negative ions were scanned alternatively, the collision gas was high-purity argon, and the sheath gas was nitrogen, 40 Arb. A Waters T3 chromatographic column was used, the aqueous phase was a 0.01% formic acid-water solution, the organic phase was a 0.1% formic acid acetonitrile, and the injection volume added to the automatic sampler was 5.00 μL. Standards were analyzed to generate a standard curve, and the sample was treated with methanol containing 0.1% formic acid (Aladdin, Shanghai, China) prior to performing the assay.

Hematoxylin and eosin staining

At 8 weeks post-behavioral test, the rats were deeply anesthetized with 2% isoflurane and perfused first with saline and then with 4% PFA (Servicebio) through the left ventricle. The brain was removed from the skull and post-fixed in 4% PFA, then dehydrated, embedded in paraffin, and cut into 5-μm-thick slices. For HE staining, slices were dewaxed with xylene and then ethanol. Next, the slices were stained with hematoxylin and eosin (HE; Servicebio) for 5 minutes, rinsed with running water, dehydrated, cleared with anhydrous ethanol and xylene, and sealed with neutral gum. Images were acquired using an optical microscope (Olympus).

Immunohistochemistry

Tissue slices were prepared as described above. For each rat, one out of every ten sections was chosen for immunostaining. Sections were deparaffinized, the antigen was retrieved with citrate buffer (Servicebio), and the endogenous peroxidase was removed with 3% hydrogen peroxide solution (ANNJET, Dezhou, China). The sections were then incubated with 3% bovine serum albumin (Servicebio) to block nonspecific binding and incubated overnight at 4°C with an antibody to tyrosine hydroxylase (TH 1:1000, Abcam, Cambridge, UK, Cat# ab112; RRID: AB_297840), a marker of dopaminergic neurons. Sections were incubated with horseradish peroxidase-labeled secondary antibody (1:200, Servicebio, Cat# GB23303, RRID: AB_2811189) for 30 minutes at 37°C. 3,3′-Diaminobenzidine (DAB) (Servicebio) was used as chromogenic agent. Then, sections were counterstained with hematoxylin for 1 minute, dehydrated, cleared, and sealed. The steps were performed as described above, and images were acquired with an optical microscope (Olympus). The number of TH-immunoreactive neurons on both sides (lesioned and non-esioned) of the SN from four to six sections per rat was counted under the microscope using a blinded approach (Liu et al., 2010). Since this PD model is a unilateral damage model, the survival rate of TH-positive cells was obtained by calculating the ratio of TH-positive cells on the lesioned side to TH-positive cells on the non-lesioned side, as follows: percentage of neurons (%) = TH numbers on the lesioned side/TH numbers on the non-lesioned side × 100 (Yu et al., 2021).

Immunofluorescence staining

To observe the colocalization of PKH26 and TH or Iba-1, frozen sections (see above) were stained with TH and Iba-1 (1:1000, Wako, Tokyo, Japan, Cat# 019-19741, RRID: AB_839504) primary antibodies, a fluorescent secondary antibody, and 4′,6-diamidino-2-phenylindole (DAPI) for nuclear staining. To detect Iba-1 expression in the SN, TH/Iba-1 homologous double labeling was performed. After adding the TH primary antibody and then the secondary antibody, FITC-TSA (Servicebio) was added, and the sections were incubated in the dark for 10 minutes. After antigen retrieval with citrate buffer (Servicebio), sections were incubated with Iba-1 primary antibody at 4°C for 12 hours and Cy3-conjugated secondary antibody (donkey, 1:250; Servicebio, Cat# GB21403, RRID: AB_2818951) in the dark at room temperature for 50 minutes, and DAPI (Invitrogen, Carlsbad, CA, USA) was used to stain the nuclei. The number of Iba-1-positive microglia was automatically determined using a fluorescent microscope (Nikon, Tokyo, Japan) with the NIS Elements Software (version 4.2, Nikon), and the defined area contained the entire SN on both sides (Wang et al., 2020). The percentage of microglia (%) = Iba-1-positive cells on the lesioned side/Iba-1-positive cells on the non-lesioned side × 100.

In addition, we evaluated the microglial response using a four-point categorical rating scale developed by Colburn et al. (1997), based on morphological and immunoreactivity changes, in a blinded fashion. Under low (100×) and medium (200×) magnification, four to six sections from each rat were surveyed to obtain a score according to the following criteria: unperturbed, extensively ramified microglia were recorded as baseline staining (•), well-ramified microglia were considered a mild response (+), less ramified microglia at an increased density were considered a moderate response (+ +), and short, bold projections of microglia, densely arranged and overlapping, were considered an intense response (+ + +).

TUNEL assay

To further observe damage to SN neurons, PBS containing 0.1% Triton-X 100 was used to permeabilize cell membranes. After the addition of TUNEL reaction solution (Roche, Mannheim, Germany), the cells were incubated at 37°C for 2 hours, then sealed with bovine serum albumin at room temperature for 30 minutes, followed by incubation with a TH primary antibody and then a fluorescent secondary antibody. Nuclei were stained with DAPI. The green fluorescein-labeled dopaminergic neurons and red fluorescein-labeled DNA were observed and measured under a fluorescence microscope (Nikon) as described above. Damaged dopaminergic neurons were identified by double immunofluorescence staining for TUNEL and TH ($TUNEL^+/TH^+$). The damage rate (%) = the number of damaged neurons/total number of neurons ×100.

Microglia-conditioned media-induced neurotoxicity and Exo treatment

To establish an *in vitro* neuroinflammatory cell model, SH-SY5Y neurons were induced with conditioned media from BV2 microglia which stimulated with lipopolysaccharide (LPS; Sigma) and adenosine triphosphate (ATP; Aladdin). First, BV2 cells were treated with LPS (1 μg/mL), ATP (5 mM), or LPS (1 μg/mL) + ATP (5 mM) for 3, 6, 18, and 24 hours. Then, the conditioned medium was harvested and centrifuged at 800 × *g* for 5 minutes to remove the cellular debris, after which it was added to the SH-SY5Y cells. The neurotoxicity to SH-SY5Y cells was determined by cell viability assay, and the appropriate concentration and time of LPS, ATP in BV2 cells were chosen for the *in vitro* model.

For Exos treatment, Exos (0, 25, 50, 75, and 100 μg/mL) were first added to normally cultured BV2 cells for 6, 12, 24, and 48 hours to determine whether they were toxic. After determining a nontoxic concentration of Exos, BV2 cells were pretreated with Exos (0, 25, 50, 75, and 100 μg/mL) for 6 hours and then stimulated with LPS (1 μg/mL) + ATP (5 mM) for 3 hours (as described above). Then, the conditioned medium from Exos-pretreated BV2 cells was collected and transferred to SH-SY5Y cells for 18 hours, followed by performing a SH-SY5Y cell viability assay.

***In vitro* uptake of PKH26-labeled Exos**

To determine whether the Exos can be taken by BV2 cells, PKH26-labeled Exos were first added to normally cultured BV2 cells for 1, 3, 6, 12, 24, and 48 hours, and also to LPS/ATP-stimulated BV2 cells for 24 hours. Then, the cells were fixed with paraformaldehyde and sealed with a sealing agent containing DAPI. Images were taken with a confocal microscope.

CCK8 cell viability assay

The viability of BV2 cells treated with Exos and SH-SY5Y cells treated with LPS/ATP-induced BV2 conditioned media (with or without Exos pretreatment) was measured using a cell counting kit-8 (CCK8, Solarbio, Beijing, China). The SH-SY5Y or BV2 cells were seeded in a 96-well culture plate. The blank wells (culture medium for SH-SY5Y or BV2 cells), control wells (normal cells), and experimental wells were designated. After LPS/ATP or Exos treatment, the supernatant was discarded. Then, 100 μL fresh medium for SH-SY5Y or BV2 cells (DMEM/F12, same as above) containing 10 μL CCK8 solution was added to each well, and the cells were incubated for 2.5 hours, after which the absorbance at 450 nm was measured using a microplate reader (Thermo Fisher Scientific). Cell viability was calculated based on the following formula: cell viability (%) = (Absorbance value$_{\text{experimental well}}$ – Absorbance value$_{\text{blank well}}$)/(Absorbance value$_{\text{control well}}$ – Absorbance value$_{\text{blank well}}$) × 100.

Scanning electron microscopy

BV2 cells grown on climbing films were fixed in 2.5% glutaraldehyde (Structure Probe, West Chester, PA, USA) for 2–4 hours, rinsed with phosphate-buffered saline three times, and fixed in 1% osmic acid (Innochem, Beijing, China) at 4°C for 2 hours. After rinsing with double-distilled water three times, the cells were dehydrated with an ethanol gradient, treated with isoamyl acetate (Innochem), and dried in a Critical Point Dryer (Quorum, Manchester, UK) by heating to 15°C for 10 minutes, and then to 35°C. After coating with an ion sputter coater (Cressington, Watford, UK), images were collected with a scanning electron microscope (Hitachi).

Enzyme-linked immunosorbent assay

The interleukin-1β (IL-1β) and interleukin-18 (IL-18) concentrations in the BV2 growth medium were assayed by enzyme-linked immunosorbent assay (ELISA). First, 10 μL standards and 10 μL samples were added to microplate wells. Then, according to the kit instructions (Multi Sciences, Hangzhou, China), 50 μL first reagent and 100 μL horseradish peroxidase-labeled streptavidin were added to each well. 3,3′,5,5′-Tetramethylbenzidine (TMB; 100 μL) was used as a chromogenic agent. The absorbance at 450 nm and 570 nm was assayed with a microplate reader (Thermo Fisher Scientific). The corrected absorbance value (Absorbance$_{450\text{ nm}}$ – Absorbance$_{570\text{ nm}}$) was normalized to controls.

High-throughput sequencing of hucMSCs-Exos microRNAs
Total RNA from Exos was extracted and purified using an miRNeasy Mini Kit (Qiagen, Dus, Germany) according to the manufacturer's instruction. A small RNA library was constructed using SMARTer Stranded Total RNA-Seq kit (Takara, Osaka, Japan). The library was sequenced using an Illumina Hiseq 2500 high-throughput sequencer (Illumina, San Diego, California). Sequence alignment of the clean was performed using the Silva, GtRNAdb, Rfam, and Repbase databases and Bowtie software V 1.0 (https://bowtie-bio.sourceforge.net/index.shtml; Langmead et al., 2009) to identify known microRNAs (miRNAs). Target genes were predicted using miRanda V3.3a (http://cbio.mskcc.org/microrna_data/miRanda-aug2010.tar.gz; Enright et al., 2003; Betel et al., 2008) and RNAhybrid V2.1.1 (https://bibiserv.cebitec.uni-bielefeld.de/rnahybrid; Rehmsmeier et al., 2004; Krüger and Rehmsmeier, 2006).

hucMSC-Exo protein spectrum sequencing
Label-free protein spectrum sequencing of Exos peptides was performed by liquid chromatography-tandem mass spectrometry (LC-MS/MS) (Q Extractive HF-X mass spectrometer, Thermo Fisher Scientific). The sequencing results were compared with the UniProt database (http://www.uniprot.org/).

The peptide signals obtained from the LC-MS data were identified and corrected using Proteome Discoverer software version 2.2 (Thermo Fisher Scientific). The results were then checked for quality, quantity, and integration to obtain the proteomic data.

Bioinformatics analysis
Gene ontology (GO) functional annotation was performed using the David online database (https://david.ncifcrf.gov), repeated measures analysis of variance followed by Tukey's *post hoc* test and Kyoto Encyclopedia of Genes and Genomes (KEGG) signal pathway enrichment analysis was also performed (http://www.genome.jp/kegg/). A protein-protein interaction (PPI) network containing the top 100 proteins was constructed using the String database (https://cn.string-db.org).

Statistical analysis
No statistical methods were used to predetermine sample sizes; however, our sample sizes are similar to those reported in a previous publication (Chen et al., 2020). Repeated measures analysis of variance followed by Tukey's *post hoc* test and one-way analysis of variance followed by the least significant difference (LSD) test were used for data analysis using SPSS 20.0 (IBM, Armonk, NY, USA). All data are expressed as the mean ± standard deviation (SD). $P < 0.05$ was considered statistically significant.

Results

Typical characteristics of hucMSCs and hucMSC-Exos
To verify the identity of the isolated mesenchymal stem cells, we observed cell morphology, performed trypan blue staining and cell counts to plot the cell growth curve, and performed flow cytometry analysis of cell surface markers. The cells isolated from the human umbilical cords grew in parallel or spiral shapes (**Figure 1A**). The cells displayed logarithmic growth followed by a static growth period, which is in line with the growth pattern of stem cell populations (**Figure 1B**). More than 99.9% of the cells expressed the MSC surface antigens CD73, CD105, and CD90, while less than 0.5% of the cells expressed the hematopoietic stem cell antigens CD34 and CD45 and the human leukocyte antigen (HLA)-DR (**Figure 1C**). Red calcium deposition was observed during osteogenic induction, a large number of the oil red O–positive lipid droplets were observed during adipogenic induction, and the deposition of acid mucopolysaccharide with positive Alcian blue staining was observed during chondrogenic induction, suggesting multiple differentiation potential (**Figure 1D**). The above results confirmed that the isolated cells were indeed mesenchymal stem cells.

To identify Exos isolated from hucMSCs, transmission electron microscopy, NTA, and western blot were used to assess cell morphology, particle size, and surface markers, respectively. We found that the extracted Exos had a cup-shaped, cupholder-shaped, or biconcave discoid-shaped double-layer membrane structure **(Figure 1E**). Overall, 98.1% of the particles were 110.1 nm in size, which is within the normal range for Exos particle size (30–150 nm) (**Figure 1E**). The Exos were positive for the Exos markers CD63, TSG101, and Alix, and negative for the organelle protein calnexin (**Figure 1E**). These results confirmed that the Exos were appropriately isolated.

HucMSC-Exos colocalize with DA neurons and microglia in the SN, improve motor function recovery, and increase the concentration of DA and its metabolites in the striatum of PD model rats
An outline of the *in vivo* experiment is shown in **Figure 2A**. To investigate whether hucMSC-Exos can cross the BBB to enter the damaged SN, PKH26-labeled Exos were injected via the tail vein or into the lateral ventricle of PD model rats for 24 hours. Immunofluorescence staining showed that hucMSC-Exos colocalized with damaged DA neurons (**Figure 2B**) and microglia (**Figure 2C**) in the lesioned SN, suggesting that hucMSC-Exos can be taken up by both cell types. We noticed that the microglia in the control group were unperturbed and extensively ramified, while the microglia in the other three groups exhibited short and bold projections, reflecting microglia activation. The percentage of neuronal loss and microglia activation in the PD model at 3 weeks are shown in **Additional Figure 1**.

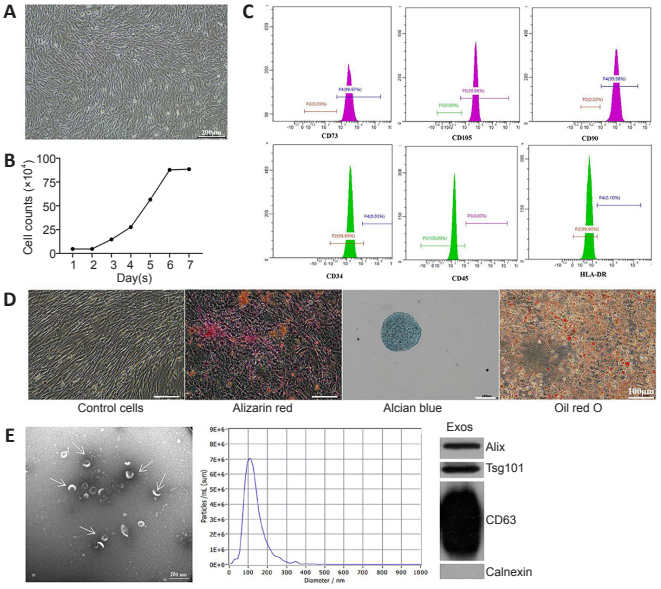

Figure 1 | Typical characteristics of hucMSCs and hucMSC-Exos.
(A) Morphology of hucMSCs. Scale bar: 200 μm. (B) hucMSCs growth curve. The cells displayed a logarithmic growth followed by a static growth period, which is in line with the growth of stem cell populations. (C) hucMSCs surface antigens were assayed by flow cytometry. The cells were positive for the MSC-specific cell surface antigens CD73, CD105, and CD90 and negative for the hematopoietic stem cell antigens CD34, CD45, and HLA-DR. (D) Three-directional differentiation of hucMSCs. Adipogenic, osteogenic and chondrogenic differentiation were detected by oil red O, Alizarin red, and Alcian blue staining, respectively. Scale bars: 100 μm. (E) Typical characteristics of Exos: transmission electron microscope (TEM) image (left), particle size shown by nano-particle size tracking analysis (NTA) (middle), positive expression of Exos markers including Alix, Tsg 101, and CD63, and negative expression of organelle protein calnexin shown by western blotting (right). Scale bar: 200 nm. Exos: Exosomes; HLA: human leukocyte antigen; hucMSCs: human umbilical cord mesenchymal stem cells.

To investigate the effect of hucMSC-Exos on behavior in a 6-OHDA-induced rat model of PD, we assessed APO-induced rotation at 2, 4, 6, and 8 weeks after Exos injection. Compared with the 6-OHDA group, the rotational number in the Exos-LV group decreased significantly from 6 weeks, and that in the Exos-T group decreased significantly from 4 weeks after injection ($P < 0.01$), and both continued until 8 weeks after injection ($P < 0.01$). These findings suggest that administration of Exos by both injection methods improved behavior in PD model rats, and there was no significant difference between the two injection methods (**Figure 2D**).

Next, high performance liquid chromatography-mass spectrometry (HPLC-MS) was used to determine the concentrations of DA, 5-HT, and their metabolites. The molecular structure of all analytes is shown in **Figure 2E**. 3,4-Dihydroxyphenyl acetic acid (DOPAC) and homovanillic acid (HVA) are metabolites of DA, 5-HT concentration is related to coordinated movement, and 5-HIAA is a metabolite of 5-HT. The HPLC-MS results showed that, compared with the 6-OHDA group, the concentrations of DA, 5-HIAA ($P < 0.01$), DOPAC, HAV, and 5-HT ($P < 0.05$) in both injection groups were significantly increased, and there was no significant difference between Exos-T and Exos-LV groups ($P > 0.05$; **Figure 2F**).

HucMSC-Exos reduce damage to DA neuron in the substantia nigra of PD model rats
To investigate the protective effect of hucMSC-Exos on DA neurons in the lesioned SN in PD model rats, HE and immunohistochemistry staining were performed. HE staining showed that, in the control group, most neurons were arranged in a regular pattern and contained large, round nuclei. The neuronal architecture was clearly visible and morphologically intact. In the 6-OHDA group, the cells were disarranged. Some neurons were shrunken, the cells stained darkly, and the boundary between the nucleus and cytoplasm was unclear. The interstitial space was relatively loose, and many vacuoles could be observed in the SN. Compared with 6-OHDA-treated rats, the pathological changes were reduced in the Exos-LV and Exos-T groups (**Figure 3A**). TH immunoreactivity analysis (**Figure 3B**) showed that 6-OHDA treatment decreased the number of TH neurons in the lesioned SN, while the number of TH neurons in the Exos-LV and Exos-T groups was significantly increased ($P < 0.001$; **Figure 3C**).

To further determine the effect of hucMSC-Exos on DA neurons in the PD rat model, TH and TUNEL double immunofluorescence staining was used to assess damage to TH-positive neurons. The results showed that TH and TUNEL double-positive cell numbers were significantly increased in 6-OHDA-treated rats and decreased in Exos-LV and Exos-T rats (both $P < 0.001$). There was no significant difference in the number of TH and TUNEL double-positive cells between the Exos-LV and Exos-T groups (**Figure 3D** and **E**). These data suggest that hucMSC-Exos reduced the damage to DA neurons caused by 6-OHDA.

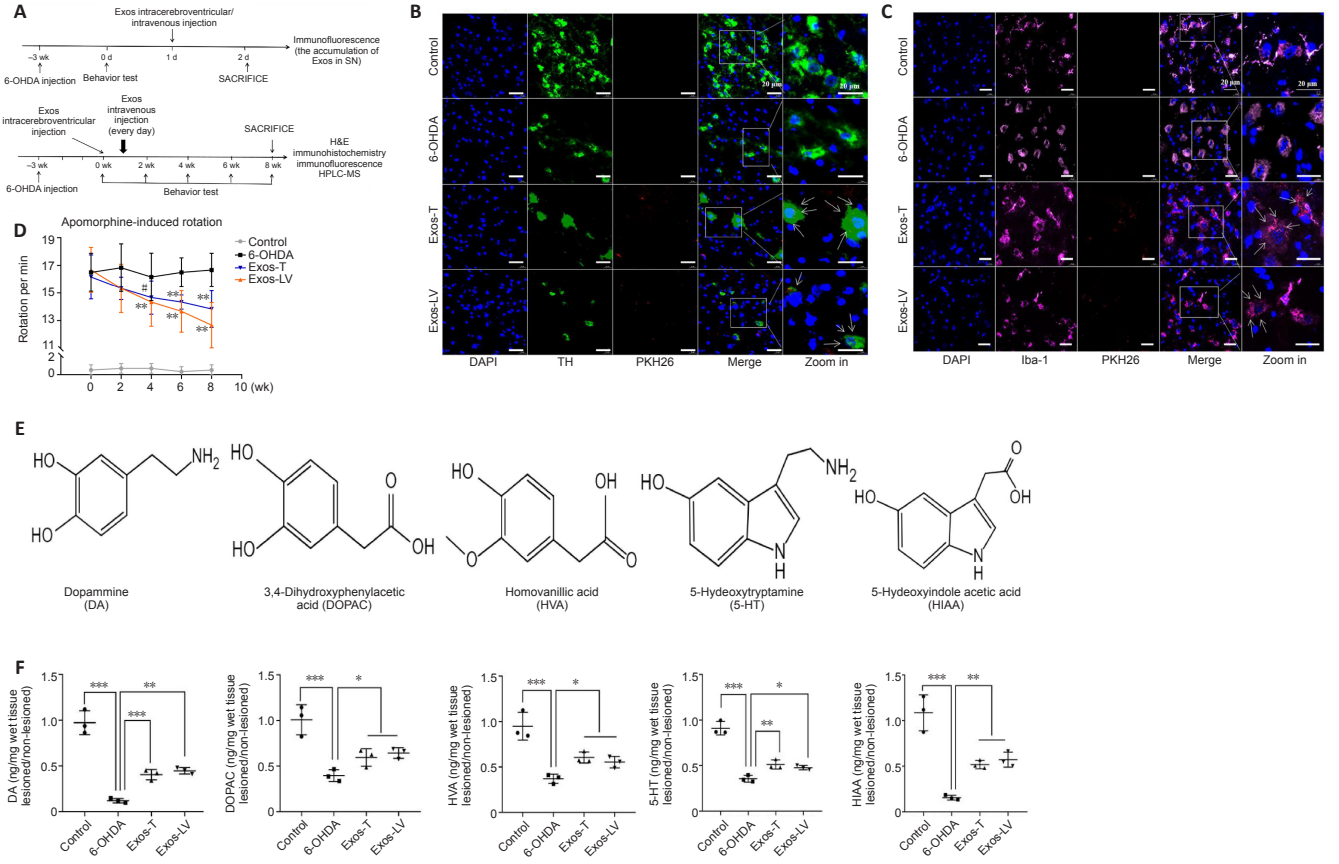

Figure 2 | **HucMSC-Exos co-localized with DA neurons and microglia in the lesioned substantia nigra improved behavior, and increased the concentrations of DA and its metabolites in lesioned striatum of PD model rats.**

(A) Schematic diagram of the *in vivo* experiment. (B) Colocalization of Exos (red) and DA neurons (green), identified by TH expression, in the lesioned substantia nigra (n = 3). (C) Colocalization of Exos (red) and microglia (pink), identified by Iba-1 expression, in the lesioned substantia nigra. Blue indicates DAPI-stained nuclei (n = 3). The arrow indicates Exos, and the box indicates the enlarged area. Scale bars: 20 μm in B and C. (D) Intraperitoneal injection of APO (0.5 mg/kg) induced rotation in rats. Rotation was assessed 21 days after 6-OHDA injection (before Exos injection, i.e., 0 week) and 2, 4, 6, and 8 weeks after Exos injection. 6-OHDA group: injection of 6-OHDA without Exos; control group: no injection of 6-OHDA or Exos; Exos-LV group: 6-OHDA + Exos injected into the lateral ventricle; Exos-T group: 6-OHDA + Exos injected into the tail vein. $^{**}P < 0.01$, *vs.* 6-OHDA group before injection (0 week), $^{\#}P < 0.01$, *vs.* before injection (0 week) (n = 6; repeated measures analysis of variance followed by Tukey's *post hoc* test). (E) The chemical structure of all analytes including DA, DOPAC, HVA, 5-HT, and HIAA. (F) The levels of the metabolites were assayed by HPLC-MS. All data are shown as the mean ± SD. $^{*}P < 0.05$, $^{**}P < 0.01$, $^{***}P < 0.001$ (n = 3; one-way analysis of variance followed by least significant difference test). Exos-T and Exos-LV indicate 6-OHDA-induced PD models treated with Exos injection through the tail or lateral ventricle, respectively. 6-OHDA: 6-Hydroxydopamine; APO: apomorphine; DA: dopamine; DAPI: 4′,6-diamidino-2-phenylindole; Exos: exosomes; HPLC-MS: High performance liquid chromatography-mass spectrometry; hucMSCs-Exos: human umbilical cord mesenchymal stem cells derived exosomes; Iba-1: Ionized calcium binding adapter molecule 1; PD: Parkinson's disease; TH: tyrosine hydroxylase.

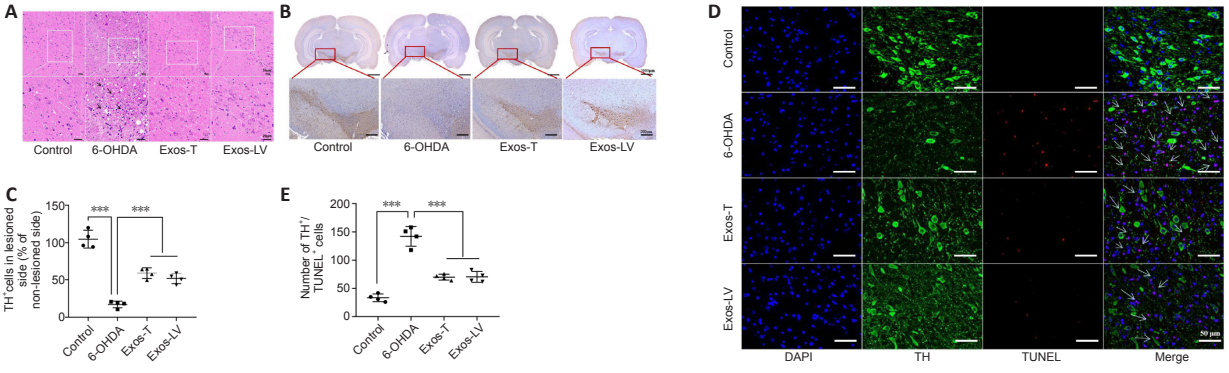

Figure 3 | **HucMSC-Exos reduces the damage to DA neuron in the substantia nigra of PD model rats.**

(A) HE staining. Arrows indicate areas where neuronal loss and morphological changes were observed. The rectangle indicates the location of the damage. Compared with the control group, cells in the 6-OHDA group were disarranged, some neurons were shrunk, and severe structural damage could be seen. These pathological changes were not apparent in the Exos-T and Exos-LV groups. Scale bars: 20 μm. (B) Representative TH immunohistochemical staining of the substantia nigra. The left side was the damaged side, and the right side was the undamaged side. Scale bars: 2000 μm in the first row, 200 μm in the second row. (C) TH^+ cells. (D) TH (green) and TUNEL (red) immunoreactivity in neurons in the substantia nigra. Blue indicates DAPI-stained nuclei. Scale bars: 50 μm. (E) Quantification of $TUNEL^+$ and TH^+ cells. Arrows indicated neurons positive for TUNEL staining and TH expression, and the box represents the enlarged area. All data shown in C and E are shown as the mean ± SD. $^{***}P < 0.001$ (n = 4; one-way analysis of variance followed by the least significant difference test). Exos-T and Exos-LV indicate 6-OHDA-induced PD models treated with Exos injection through the tail or lateral ventricle, respectively. 6-OHDA: 6-Hydroxydopamine; DA: dopamine; DAPI: 4′,6-diamidino-2-phenylindole; Exos: exosomes; HE: hematoxylin-eosin; hucMSCs-Exos: human umbilical cord mesenchymal stem cells derived exosomes; PD: Parkinson's disease; TH: tyrosine hydroxylase; TUNEL: terminal deoxynucleotidyl transferase mediated dUTP Nick-end labeling.

HucMSC-Exos reduce microglial activation in the substantia nigra of PD model rats

The effect of hucMSC-Exos on microglial activation in the lesioned SN was determined by TH and Iba-1 double immunofluorescence staining. We found that Iba-1–positive microglia in the control group had long and thin branches, while the 6-OHDA group exhibited a greater number of Iba-1–positive cells, as well as shorter and thicker branches. Compared with the 6-OHDA group, in both the Exos-LV and the Exos-T groups the microglial morphology was more like that seen in the control group, and the microglia had thinner branches (**Figure 4A**). In addition, the number of microglia was significantly decreased (*P*

< 0.001; **Figure 4B**). These data suggest that hucMSC-Exos inhibited microglial activation. Rats in the control group exhibited no microglial activation, while in the 6-OHDA group three out of four rats exhibited an intense microglial response, and rats in the Exos-T and Exos-LV groups exhibited mild to moderate microglia responses (**Table 1**).

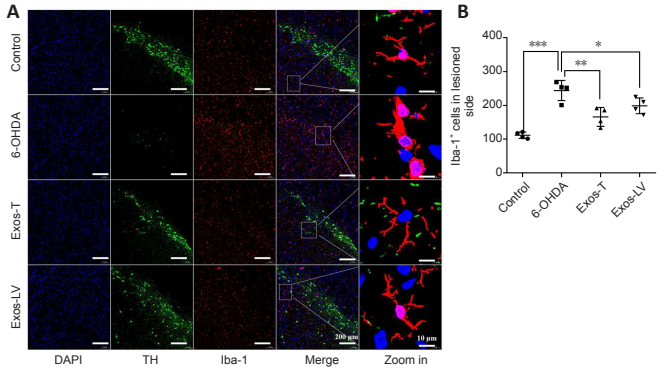

Figure 4 | HucMSC-Exos reduces microglial activation in the substantia nigra of PD model rats.
(A) Iba-1 (red) expression in the substantia nigra of rats from each group. Blue indicates DAPI-stained nuclei, and green (TH) indicates the substantia nigra region. Scale bars: 200 μm in the DAPI, TH, and Iba-1-stained images and the merge column and 10 μm in the last column. (B) Quantification of Iba-1 expression. The box indicates the enlarged area. All data are shown as the mean ± SD. *P < 0.05, **P < 0.01, ***P < 0.001 (n = 4, one-way analysis of variance followed by the least significant difference test). Exos-T and Exos-LV indicate the 6-OHDA-induced PD model treated with Exos injection through the tail or lateral ventricle, respectively. 6-OHDA: 6-Hydroxydopamine; DAPI: 4′,6-diamidino-2-phenylindole; Exos: exosomes; hucMSCs-Exos: human umbilical cord mesenchymal stem cells derived exosomes; Iba-1: ionized calcium binding adapter molecule-1; PD: Parkinson's disease; TH: tyrosine hydroxylase.

Table 1 | Microglial responses in the SN

Group	*n*	Microglia response
Control	4	•
6-OHDA	4	+ + +
		+ + +
		+ +
		+ + +
Exos-T	4	+
		+
		+ +
		+
Exos-LV	4	+ +
		+
		+
		+

Baseline "resting" morphology (•), and mild (+), moderate (+ +), and intense responses (+ + +); Exos-T and Exos-LV indicate the 6-OHDA-induced PD model treated with Exos injection through the tail or lateral ventricle, respectively. All scores pertain to the lesioned side. 6-OHDA: 6-Hydroxydopamine; Exos: exosomes; SN: substantia nigra.

HucMSC-Exos are taken up by BV2 cells and attenuate the decrease in SH-SY5Y cell viability induced by BV2 conditioned medium

To prepare an *in vitro* neuroinflammatory cell model, SH-SY5Y and BV2 cells were selected. Both of them grew well and proliferated actively, and the growth curves were consistent with the cell growth characteristics of these two cell lines.

The morphology of the SH-SY5Y (**Figure 5A**) and BV2 (**Figure 5B**) cells and their corresponding cell growth curves are shown. Spent medium from BV2 cells induced with LPS and ATP was added to SH-SY5Y cells, and SH-SY5Y cell viability was assessed by CCK8 assay. We found that conditioned medium from BV2 cells induced with 1 μg/mL LPS and 5 mM ATP for different time periods significantly reduced SH-SY5Y cell viability to 50% at 3 hours, and these conditions were chosen for the *in vitro* model (**Figure 5C**).

To determine whether Exos have a protective effect on injured neurons *in vitro*, Exos uptake by BV2 cells was first observed by confocal microscopy. Exos were taken up in small amounts by normal BV2 cells at 1 hour and in large amounts at 3 hours and later (**Figure 5D**). Exos were also taken up by BV2 after drug intervention at 24 hours, and bright field microscopy showed that the Exos entered the interior of the cells (**Figure 5D**). Furthermore, confocal microscopy with 2.5D and 3D scanning confirmed that the Exos entered the nucleus at 3 hours (**Figure 5D**).

To assess the protective effect of Exos on the neuroinflammatory cell model, we first established a time-concentration curve for the activity on Exos on normal BV2 cells. Exos at 0–100 μg/mL did not affect BV2 cell viability for 48 hours (**Figure 5E**), which suggested that the Exos had no toxicity for normal BV2 cell. Conditioned medium from BV2 cells pretreated with Exos at 50–100 μg/mL and stimulated with LPS and ATP significantly increased SH-SY5Y viability compared with condition medium from BV2 cells that were stimulated but not pretreated (P < 0.05). There was no significant difference in the results between 75 and 100 μg/mL Exos (P > 0.05; **Figure 5F**). Thus, 75 μg/mL Exos was selected for use in subsequent experiments. These data suggest that Exos protect neurons by inhibiting activation of LPS+ATP-induced microglia.

HucMSC-Exos decrease IL-1β and IL-18 secretion and prevent the adoption of pyroptosis-associated morphology by BV2 cells

To further investigate the effect of Exos on a BV2 cell model of neuroinflammation, ELISA and scanning electron microscopy were used. The ELISA results showed that IL-1β and IL-18 secretion increased significantly when BV2 cells were stimulated with LPS and ATP, and pretreatment with Exos significantly inhibited this effect (both P < 0.001; **Figure 6A**).

Cell swelling and the loss of cell membrane integrity are the main characteristics of pyroptosis. The scanning electron microscopy results showed that cell morphology in the control group was normal, and the cell contours were clear. In the LPS + ATP group, the cell morphology was irregular, swollen, and enlarged, and cells were attached to the climbing films. Vesicles generated by cytoplasmic overflow were observed, which indicated that membrane integrity was disrupted. Pretreatment with Exos decreased the number of vesicles and prevented the observed changes in cell morphology (**Figure 6B**).

MiRNA sequencing, protein spectrum sequencing, and bioinformatics analysis of hucMSC-Exos

To determine what miRNAs and proteins are contained in hucMSCs-Exos, high-throughput miRNA sequencing and mass spectrometry-based protein sequencing by LC-MS/MS were performed. We identified 616 miRNAs (associated with 14,235 target genes) and 667 proteins in Exos. MiR-7, miR-125-5p, miR-122-5p, miR-126-3p, and miR-199-3p were the most abundant miRNAs. GO annotation of these miRNAs showed that they are involved in Cellular Component (CC), Molecular Function (MF), and Biological Process (BP) (**Figure 7A**). KEGG analysis (**Figure 7B**) and PPI network analysis (**Figure 7C**) of the top 100 proteins found in the Exos revealed three subsets were in PPI networks and some signaling pathways related to inflammation or immunity such as Leukocyte transendothelial migration, PI3K-Akt. In addition to the above miRNAs, miR-423-5p, miR-150-5p, miR-34a-5p were associated with the enriched pathways.

Discussion

Many drugs have a limited effect on the brain because they cannot effectively cross the BBB. Exos not only exist in a variety of bodily fluids (Pan and Johnstone, 1983) and cells and contain a range of biological information (Valadi et al., 2007), they are also small and non-immunogenic, which is advantageous for intercellular communication. Although studies have shown that intravenously injected Exos are absorbed by the liver, spleen, lung (Imai et al., 2015), pancreas, and gastrointestinal tract (Wiklander et al., 2015) to varying degrees, they also home to and target damaged tissues (Perets et al., 2019). In addition, Exos have been shown to carry α-synuclein siRNA (Cooper et al., 2014), shRNA (Izco et al., 2019), DA, and catalase (Qu et al., 2018) to brain cells in patients with PD, and can therefore be considered an invisible nanocarrier of PD drugs. hucMSCs can differentiate into DA cells (Datta et al., 2011; Meng et al., 2016) and strongly inhibit inflammation (Bárcia et al., 2015). Exos extracted from stem cells survive longer, have lower immunogenicity, contain effective stem cell components, and are more advantageous than Exos derived from other cell sources and than stem cell therapy alone.

In this study, we found that hucMSCs-Exos have a therapeutic effect in PD model rats. First, hucMSCs were obtained by primary culture, and their identity was confirmed by analyzing morphology, growth, and three-directional differentiation (Dominici et al., 2006). Next, Exos were extracted from the cell growth medium, and their identity was confirmed by analyzing morphology, particle size, and surface antigens. To investigate the ability of Exos to penetrate the BBB and exert a therapeutic effect on PD, we established a PD model using the classic catecholamine neurotoxin 6-OHDA. Exos were then labeled with PKH26 and injected into the caudal vein and lateral ventricle. The Exos were taken up by DA neurons in the damaged SN, which suggested that they penetrated the BBB and aggregated in the damaged area. Furthermore, administration of Exos improved behavior, reduced neuronal damage, and increased the concentration of DA and its metabolites in the striatum. The therapeutic effects of both injection methods were nearly the same, which proved that intravenous injection and lateral ventricular injection of Exos resulted in the same targeting and therapeutic effects.

Homeostatic imbalance of the neuron-glial network and activation or reactive gliosis of glial cells (Balasingam et al., 1994) are key factors in the occurrence and development of PD. Microglia are macrophages in the neuroectoderm, as well as the cerebral immune cells, and are more widely present in SN than in other cerebral regions (Patel et al., 2019). An increase in inflammatory factors

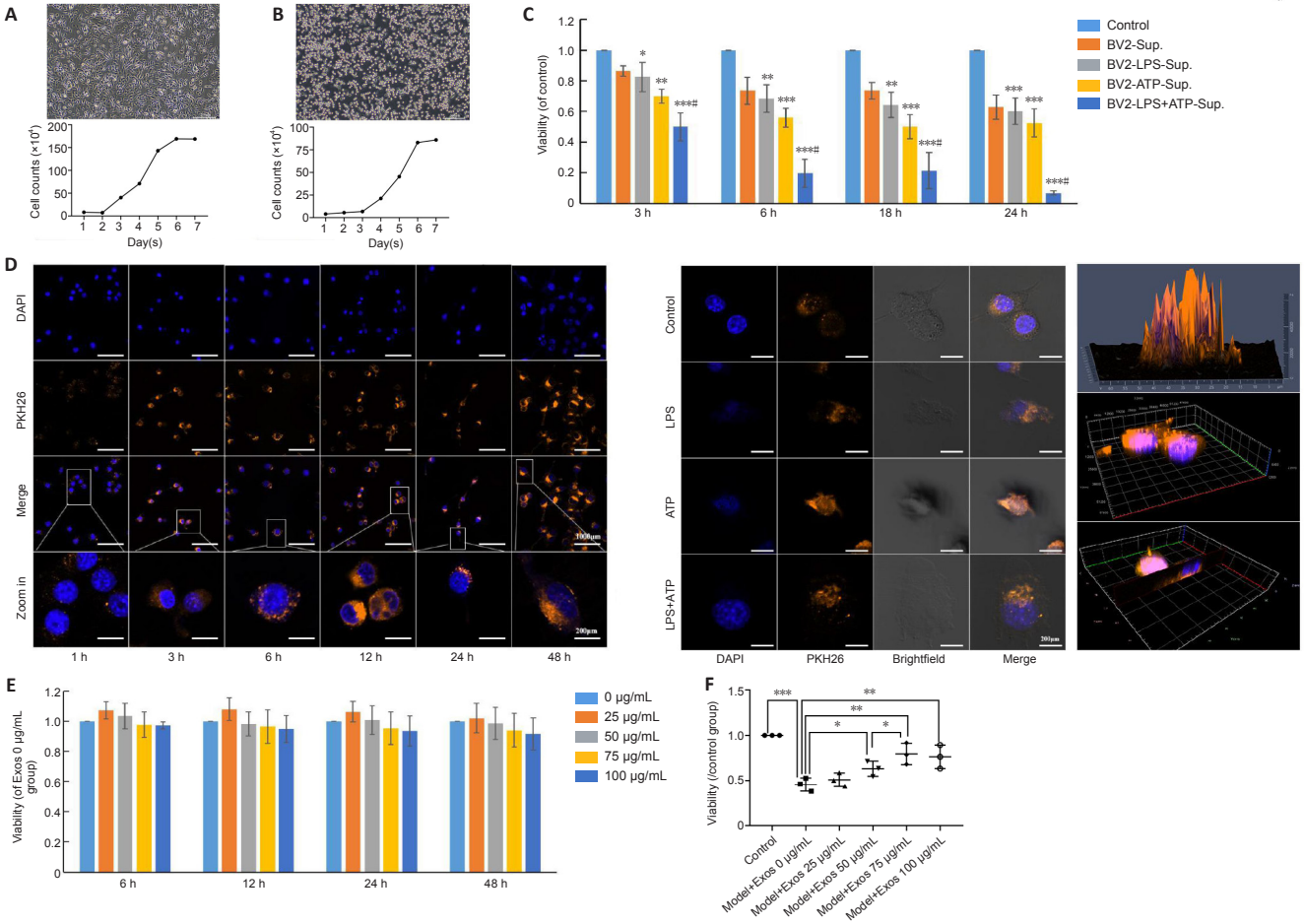

Figure 5 | HucMSC-Exos are taken up by BV2 cells and mitigate the deleterious effect on SH-SY5Y cell viability caused by growth in conditioned medium from BV2 cells stimulated with LPS.

(A, B) Morphology and growth curves of SH-SY5Y and BV2 cells. (C) Conditioned medium from BV2 cells stimulated with LPS + ATP reduced SH-SY5Y cell viability. Scale bars: 200 μm. (D) Uptake of Exos by normal BV2 cells at different time periods (left) (scale bars: 100 μm in DAPI, PKH26, and merge rows and 20 μm in the zoomed in row) and by BV2 cells stimulated with LPS and ATP at 24 hours (middle) (scale bars: 20 μm), as determined by 2.5D (upper) and 3D (middle and bottom) confocal microscopy of Exos in normal BV2 cells at 3 hours (right). Bright field and scanning microscopy showed that Exos entered the BV2 cells. Blue indicates the nuclei, and orange indicates the Exos. The box indicates the enlarged area. (E) The concentration-time curve of the effect of Exos on BV2 cell viability. The cell viability did not change significantly ($P > 0.05$) when treated with 0 to 100 μg/mL Exos for 6, 12, 24, or 48 hours. (F) The effect of conditioned medium from BV2 cells pretreated with different concentrations of Exos for 6 hours and stimulated with LPS and ATP on SH-SY5Y cell viability. Cell viability was assessed by CCK-8 assay. Three wells were assayed for each group, and the experiment was repeated three times. All data were shown as the mean ± SD. *$P < 0.05$, **$P < 0.01$, ***$P < 0.001$, *vs.* control group, #$P < 0.05$, *vs.* BV-sup group ($n = 3$, one-way analysis of variance followed by the least significant difference test). ATP: Adenosine triphosphate; CCK8: Cell Counting Kit-8; DAPI: 4′,6-diamidino-2-phenylindole; Exos: exosomes; hucMSCs-Exos: human umbilical cord mesenchymal stem cells derived exosomes; LPS: lipopolysaccharide.

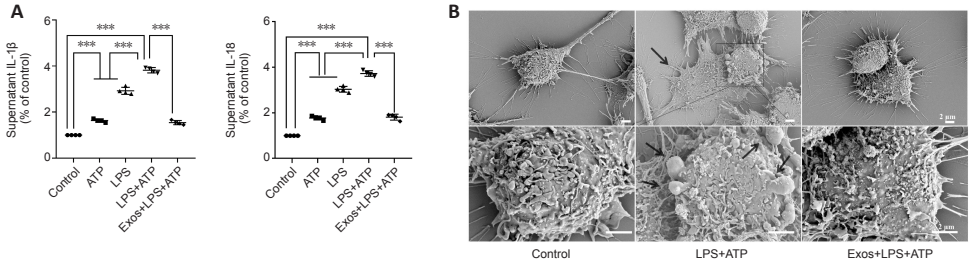

Figure 6 | HucMSC-Exos decreases IL-1β and IL-18 secretion by BV2 cells and prevents the adoption of pyroptosis-associated morphology by BV2 cells.

(A) The effect of Exos on IL-1β and IL-18 secretion by BV2 cells was assayed by enzyme-linked immunosorbent assay. (B) The effect of Exos on BV2 cell morphology as observed by scanning electron microscopy. The arrow indicates pyroptotic cells. Scale bars: 2 μm. All data are shown by mean ± SD. ***$P < 0.001$ ($n = 4$; one-way analysis of variance followed by least significant difference test). ATP: Adenosine triphosphate; ELISA: Enzyme-linked immunosorbent assay; Exos: exosomes; hucMSCs-Exos: human umbilical cord mesenchymal stem cells derived exosomes; IL-18: interleukin-18; IL-1β: interleukin-1β; LPS: lipopolysaccharide.lbeatem exerchici andi conse velessi id esequi dist mo et re pro temporum quidipsam et

(Hirsch and Hunot, 2009) such as cyclooxygenase-2 (COX-2), prostaglandins (PGs), tumor necrosis factor α (TNF-α), interleukin-3 (IL-13), and interferon γ (IFN-γ) and microglial activation play an important role in the pathology of PD. Thus, the nonsteroidal anti-inflammatory drug ibuprofen (Gao et al., 2011), as well minocycline (Du et al., 2001) and dexamethasone (Tentillier et al., 2016), which inhibit microglial activation, effectively protect DA neurons in PD model rats, confirming that neuroinflammation is correlated with PD. While investigating the anti-inflammatory mechanism of Exos in PD, we first found that Exos was taken by microglia, and then observed microglia in the SN by double immunofluorescence staining for Iba-1 and TH. In the PD model group, the microglia labeled with Iba-1 were activated, and the number of microglia was increased. However, in the Exos group the morphology of the microglia reflected that of unactivated cells, and the number of microglia was lower, suggesting that Exos may protect neurons by inhibiting microglial activation.

Exos derived from different stem cells protect myocardial function (Singla et al., 2019) and prevent intervertebral disc degeneration (Zhang et al., 2020), acute liver damage, oxygen and glucose deprivation damage (Xia et al., 2019; Liu et al., 2018), and ischemic damage (Yan et al., 2015) by inhibiting pyroptosis. Pyroptosis, as a newly discovered form of programmed inflammatory cell death, has been reported in animals (Zhang et al., 2020) and cell models of PD (Sarkar et al., 2017; Li et al., 2019). In response to the first signal—damage-associated molecular patterns (DAMPs) and pathogen-associated molecular patterns (PAMPs, e.g. LPS)—and the second signal—K^+ efflux, ATP, etc.,—the inflammatory cytokines IL-1β and IL-18 are released in to the extracellular compartment through pores formed by cleaved gasdermin D (He et al., 2018; Bedoui et al., 2020), thereby inducing and accelerating pyroptosis.

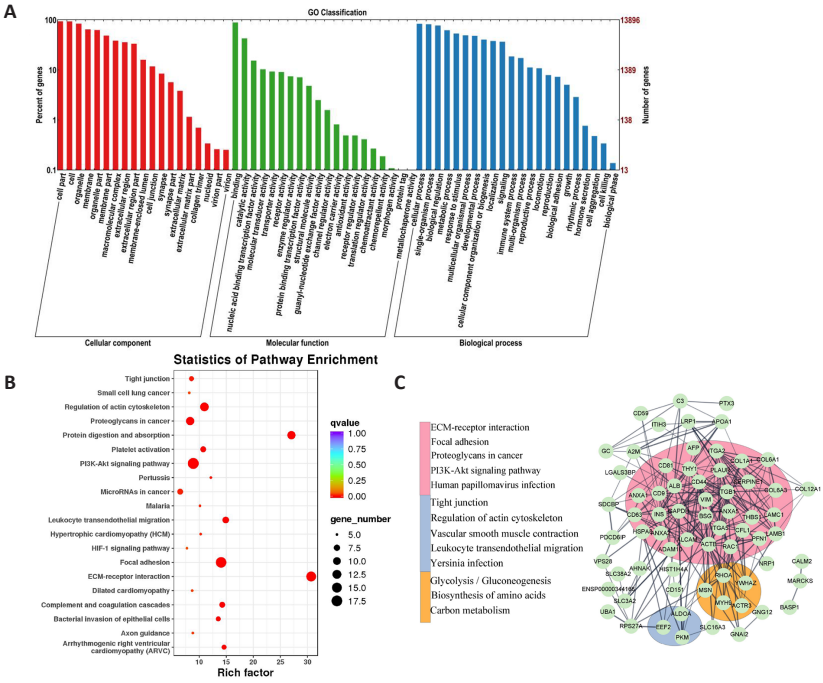

Figure 7 | MiRNA sequencing, protein spectrum sequencing, and bioinformatics analysis of Exos.
(A) GO annotation of miRNA target genes. (B) Bubble chart of KEGG analysis of the top 100 proteins. (C) PPI network constructed from the top 100 proteins. Nodes represented proteins, lines represented correlation, different colors represented different subsets, and the bar on the left side shows the top five pathways in each subset identified by the KEGG enrichment analysis. Exos: Exosomes; GO: Gene Ontology; KEGG: Kyoto Encyclopedia of Genes and Genomes; miRNA: microRNAs; PPI: protein protein interaction.

To determine the mechanisms involved in the inhibition of microglia-induced neuroinflammation, we established a classic *in vitro* neuroinflammatory model. Microglia cell line BV2 was stimulated with LPS and ATP, and the condition medium was applied to human neuroblastoma SH-SY5Y cells with DA-β-hydroxylase activity. We found that Exos were taken up by BV2 cells, and that pretreating BV2 cells with Exos significantly increased cell viability of SH-SY5Y cells grown in the conditioned medium. Furthermore, IL-1β and IL-18 secretion by BV2 cells increased significantly, and scanning electron microscopy showed that the BV2 cells were swollen and exhibited ruptured cell membranes that appeared to be leaking pyroptosis bodies and/or other intracellular substances, which is in line with the characteristics of pyroptosis (Lu et al., 2018; Chen et al., 2019; Yao et al., 2020; Luo et al., 2022). Pretreatment with Exos decreased IL-1β and IL-18 secretion, reduced cell membrane pore formation and cytoplasmic overflow, and restored the morphology of pyroptosis cells, suggesting that Exos may inhibit pyroptosis in microglia.

Many studies (Aliotta et al., 2016; Xiong et al., 2017; Vilaça-Faria et al., 2019; Wu et al., 2019; Tang et al., 2022) have suggested that Exos exerts their activity through the miRNAs or proteins that they contain, especially Exos derived from MSCs. In this study, we found that the miRNA and protein we detected in hucMSCs-Exos were involved in a variety of biological activities, including the NF-κB, PI3K/Akt, mTOR, and some immune-related signaling pathways. The PI3K/Akt signaling pathway activates both the NF-κB signaling pathway and its downstream pathways and promotes pyroptosis, as well as inhibiting autophagy mediated by PI3K/Akt/mTOR, while autophagy can inhibit the progress of pyroptosis (Shi et al., 2012; Deretic et al., 2013; **Figure 8**). Among the miRNAs identified in the Exos, miRNA-122, miRNA-125, miRNA-126, and miRNA-199 were highly expressed and confirmed to be involved in NF-κB pathway activation (Kim et al., 2012; Niu et al., 2015; Rivkin et al., 2016) and autophagy (Santovito et al., 2020) in other diseases. In particular, it has been reported that miR-7 expression is significantly decreased in brain tissues of PD patients and PD model mice (Horst et al., 2018). The reduction in miR-7 expression in the brains of PD patients and the inhibition of miR-7 function in normal mice (McMillan et al., 2017) can both lead to aggregation of α-syn, loss of DA neurons in the SN, and a reduction in the DA content of the striatum. It is speculated that these miRNAs may regulate the PI3K/Akt pathway, thereby inhibiting the downstream generation of the NF-κB/NLRP3 inflammasome, and eliminate excess NLRP3 inflammasomes by accelerating autophagy, therefore inhibiting the occurrence of pyroptosis. The exact mechanism needs to be further explored.

There were some limitations to the current study. For example, in the *in vitro* experiments, we only determined the inhibitory effects of Exos on microglia through analysis of morphology and cytokines; considering that Exos may play a role in inhibiting pyroptosis, related signals such as pyroprotein expression should be explored in future studies. In addition, although we identified some potentially significant miRNAs or proteins in Exos, we did not confirm whether they play a key role in the inhibition of neuroinflammation, and we do not fully understand their potential; thus, it is difficult to predict whether these miRNAs will be clinically useful.

In conclusion, our findings suggest that exosomes derived from human umbilical cord mesenchymal stem cells may be a valuable treatment for neurodegenerative diseases, especially PD, in the future. Although the detailed mechanism of their effects, such as the functions of the microRNAs and proteins that they contain, need to be confirmed, our findings have the potential to lead to the development of effective interventions. This study showed that hucMSCs-Exos are a promising approach for the treatment of PD and provide a theoretical basis for clinical applications in future.

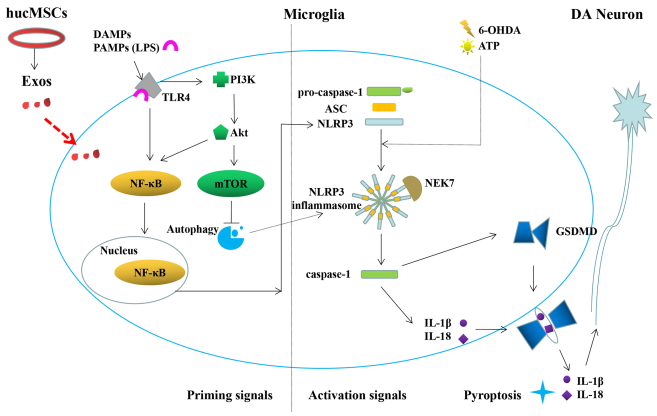

Figure 8 | Microglia pyroptosis and the therapeutic mechanism of hucMSC-Exos in PD.
Stimulation of TLR4 with LPS activates the intracellular PI3K/Akt pathway, which then activates NF-κB and mTOR, accelerating NLRP3 inflammatory corpuscle aggregation and pyroptosis. hucMSC-Exos may inhibit pyroptosis through the TLR4/NF-κB and PI3K/AKT pathway. hucMSCs-Exos: Human umbilical cord mesenchymal stem cells-exosomes; LPS: Lipopolysaccharide; mTOR: mechanistic target of rapamycin; NLRP3: NOD-like receptor thermal protein domain associated protein 3; PD: Parkinson's disease; TLR4: Toll-like receptor 4.

Author contributions: *ZXZ, YJZ, PG, RYW, LYZ, QZC, WZ, HXC, LQZ, KZ, SKF, HJX, XQC and SJA designed the study, analyzed and interpreted the data, and drafted the manuscript. ZXZ, YJZ, PG, RYW, LYZ, QZC, WZ, XQC, HXC, LQZ, KZ, and SJA conducted the experiments and analyzed the data. All authors have read and approved the final version of the manuscript.*
Conflicts of interest: *The authors declare that the study was conducted in the absence of any commercial or financial relationships that could be construed as a potential conflict of interest.*
Author statement: *This paper has been posted as a preprint on Research Square with DOI: https://doi.org/10.21203/rs.3.rs-1663711/v1, which is available from: https://assets.researchsquare.com/files/rs-1663711/v1/45906765-6cd8-4674-8456-731b93e7f221.pdf?c=1653666935.*
Data availability statement: *All relevant data are within the paper.*

References

Adams B, Nunes JM, Page MJ, Roberts T, Carr J, Nell TA, Kell DB, Pretorius E (2019) Parkinson's disease: a systemic inflammatory disease accompanied by bacterial inflammagens. Front Aging Neurosci 11:210.

Ahmed S, Kwatra M, Ranjan Panda S, Murty USN, Naidu VGM (2021) Andrographolide suppresses NLRP3 inflammasome activation in microglia through induction of parkin-mediated mitophagy in in-vitro and in-vivo models of Parkinson disease. Brain Behav Immun 91:142-158.

Aliotta JM, Pereira M, Wen S, Dooner MS, Del Tatto M, Papa E, Goldberg LR, Baird GL, Ventetuolo CE, Quesenberry PJ, Klinger JR (2016) Exosomes induce and reverse monocrotaline-induced pulmonary hypertension in mice. Cardiovasc Res 110:319-330.

Avram CM, Brumbach BH, Hiller AL (2021) A report of tamoxifen and Parkinson's disease in a US population and a review of the literature. Mov Disord 36:1238-1242.

Balasingam V, Tejada-Berges T, Wright E, Bouckova R, Yong VW (1994) Reactive astrogliosis in the neonatal mouse brain and its modulation by cytokines. J Neurosci 14:846-856.

Bárcia RN, Santos JM, Filipe M, Teixeira M, Martins JP, Almeida J, Água-Doce A, Almeida SC, Varela A, Pohl S, Dittmar KE, Calado S, Simões SI, Gaspar MM, Cruz ME, Lindenmaier W, Graça L, Cruz H, Cruz PE (2015) What makes umbilical cord tissue-derived mesenchymal stromal cells superior immunomodulators when compared to bone marrow derived mesenchymal stromal cells? Stem Cells Int 2015:583984.

Bedoui S, Herold MJ, Strasser A (2020) Emerging connectivity of programmed cell death pathways and its physiological implications. Nat Rev Mol Cell Biol 21:678-695.

Bertheloot D, Latz E, Franklin BS (2021) Necroptosis, pyroptosis and apoptosis: an intricate game of cell death. Cell Mol Immunol 18:1106-1121.

Betel D, Wilson M, Gabow A, Marks DS, Sander C (2008) The microRNA. org resource: targets and expression. Nucleic Acids Res 36:D149-153.

Brochard V, Combadière B, Prigent A, Laouar Y, Perrin A, Beray-Berthat V, Bonduelle O, Alvarez-Fischer D, Callebert J, Launay JM, Duyckaerts C, Flavell RA, Hirsch EC, Hunot S (2009) Infiltration of CD4+ lymphocytes into the brain contributes to neurodegeneration in a mouse model of Parkinson disease. J Clin Invest 119:182-192.

Cerri S, Mus L, Blandini F (2019) Parkinson's disease in women and men: what's the difference? J Parkinsons Dis 9:501-515.

Chen HX, Liang HC, Gu P, Xu BL, Xu HJ, Wang WT, Hou JY, Xie DX, Chai XQ, An SJ (2020) Exosomes derived from mesenchymal stem cells repair a Parkinson's disease model by inducing autophagy. Cell Death Dis 11:288.

Chen S, Zhou C, Yu H, Tao L, An Y, Zhang X, Wang Y, Wang Y, Xiao R (2019) 27-Hydroxycholesterol contributes to lysosomal membrane permeabilization-mediated pyroptosis in co-cultured SH-SY5Y cells and C6 cells. Front Mol Neurosci 12:14.

Chung TH, Hsu SC, Wu SH, Hsiao JK, Lin CP, Yao M, Huang DM (2018) Dextran-coated iron oxide nanoparticle-improved therapeutic effects of human mesenchymal stem cells in a mouse model of Parkinson's disease. Nanoscale 10:2998-3007.

Colburn RW, DeLeo JA, Rickman AJ, Yeager MP, Kwon P, Hickey WF (1997) Dissociation of microglial activation and neuropathic pain behaviors following peripheral nerve injury in the rat. J Neuroimmunol 79:163-175.

Cooper JM, Wiklander PB, Nordin JZ, Al-Shawi R, Wood MJ, Vithlani M, Schapira AH, Simons JP, El-Andaloussi S, Alvarez-Erviti L (2014) Systemic exosomal siRNA delivery reduced alpha-synuclein aggregates in brains of transgenic mice. Mov Disord 29:1476-1485.

Croisier E, Moran LB, Dexter DT, Pearce RK, Graeber MB (2005) Microglial inflammation in the parkinsonian substantia nigra: relationship to alpha-synuclein deposition. J Neuroinflammation 2:14.

Datta I, Mishra S, Mohanty L, Pulikkot S, Joshi PG (2011) Neuronal plasticity of human Wharton's jelly mesenchymal stromal cells to the dopaminergic cell type compared with human bone marrow mesenchymal stromal cells. Cytotherapy 13: 918-932.

Deretic V, Saitoh T, Akira S (2013) Autophagy in infection, inflammation and immunity. Nat Rev Immunol 13:722-737.

Dominici M, Blanc KL, Mueller I, Slaper-Cortenbach I, Marini F, Krause D, Deans R, Keating A, Prockop D, Horwitz E (2006) Minimal criteria for defining multipotent mesenchymal stromal cells. The International Society for Cellular Therapy position statement. Cytotherapy 8:315-317.

Du Y, Ma Z, Lin S, Dodel RC, Gao F, Bales KR, Triarhou LC, Chernet E, Perry KW, Nelson DL, Luecke S, Phebus LA, Bymaster FP, Paul SM (2001) Minocycline prevents nigrostriatal dopaminergic neurodegeneration in the MPTP model of Parkinson's disease. Proc Natl Acad Sci U S A 98:14669-14674.

Enright AJ, John B, Gaul U, Tuschl T, Sander C, Marks DS (2003) MicroRNA targets in Drosophila. Genome Biol 5:R1.

Gao X, Chen HL, Schwarzschild MA, Ascherio A (2011) Use of ibuprofen and risk of Parkinson disease. Neurology 76:863-869.

Gordon R, Albornoz EA, Christie DC, Langley MR, Kumar V, Mantovani S, Robertson AAB, Butler MS, Rowe DB, O'Neill LA, Kanthasamy AG, Schroder K, Cooper MA, Woodruff TM (2018) Inflammasome inhibition prevents α-synuclein pathology and dopaminergic neurodegeneration in mice. Sci Transl Med 10:eaah4066.

Gu P, Zhang ZX, Cui DS, Wang YY, Ma L, Geng Y, Wang MW (2012) Intracerebroventricular transplanted bone marrow stem cells survive and migrate into the brain of rats with Parkinson's disease. Neural Regen Res 7:978-984.

He M, Bianchi ME, Coleman TR, Tracey KJ, Al-Abed Y (2018) Exploring the biological functional mechanism of the HMGB1/TLR4/MD-2 complex by surface plasmon resonance. Mol Med 24:21.

Hirsch EC, Hunot S (2009) Neuroinflammation in Parkinson's disease: a target for neuroprotection? Lancet Neurol 8:382-397.

Horst CH, Schlemmer F, de Aguiar Montenegro N, Domingues ACM, Ferreira GG, da Silva Ribeiro CY, de Andrade RR, Del Bel Guimarães E, Titze-de-Almeida SS, Titze-de-Almeida R (2018) Signature of aberrantly expressed microRNAs in the striatum of rotenone-induced Parkinsonian Rats. Neurochem Res 43:2132-2140.

Imai T, Takahashi Y, Nishikawa M, Kato K, Morishita M, Yamashita T (2015) Macrophage-dependent clearance of systemically administered B16BL6-derived exosomes from the blood circulation in mice. J Extracell Vesicles 4:26238.

Izco M, Blesa J, Schleef M, Schmeer M, Porcari R, Al-Shawi R, Ellmerich S, de Toro M, Gardiner C, Seow Y, Reinares-Sebastian A, Forcen R, Simons JP, Bellotti V, Cooper JM, Alvarez-Erviti L (2019) Systemic exosomal delivery of shRNA minicircles prevents parkinsonian pathology. Mol Ther 27:2111-2122.

Kim SW, Ramasamy K, Bouamar H, Lin AP, Jiang DF, Aguiar RC (2012) MicroRNAs miR-125a and miR-125b constitutively activate the NF-κB pathway by targeting the tumor necrosis factor alpha-induced protein 3 (TNFAIP3, A20). Proc Natl Acad Sci U S A 109:7865-7670.

Krüger J, Rehmsmeier M (2006) RNAhybrid: microRNA target prediction easy, fast and flexible. Nucleic Acids Res 34:W451-454.

Langmead B, Trapnell C, Pop M, Salzberg SL (2009) Ultrafast and memory-efficient alignment of short DNA sequences to the human genome. Genome Biol 10:R25.

Li MY, Zhu XL, Zhao BX, Shi L, Wang W, Hu W, Qin SL, Chen BH, Zhou PH, Qiu B, Gao Y, Liu BL (2019) Adrenomedullin alleviates the pyroptosis of Leydig cells by promoting autophagy via the ROS-AMPK-mTOR axis. Cell Death Dis 10:489.

Liu J, Wang MW, Gu P, Ma QY, Wang YY, Geng Y, Yuan ZY, Cui DS, Zhang ZX, Ma L, Zhang BH, Zhou MG, Zhu AP (2010) Microglial activation and age-related dopaminergic neurodegeneration in MPTP-treated SAMP8 mice. Brain Res 1345:213-220.

Liu Y, Lou G, Li A, Zhang T, Qi J, Ye D, Zheng M, Chen Z (2018) AMSC-derived exosomes alleviate lipopolysaccharide/d-galactosamine-induced acute liver failure by miR-17-mediated reduction of TXNIP/NLRP3 inflammasome activation in macrophages. BioMedicine 36:140-150.

Lu H, Zhang S, Wu J, Chen M, Cai MC, Fu Y, Li W, Wang J, Zhao X, Yu Z, Ma P, Zhuang G (2018) Molecular targeted therapies elicit concurrent apoptotic and GSDME-dependent pyroptotic tumor cell death. Clin Cancer Res 24:6066-6077.

Luo X, Bao XY, Weng XZ, Bai XX, Feng Y, Huang JX, Liu SY, Jia HB, Yu B (2022) The protective effect of quercetin on macrophage pyroptosis via TLR2/Myd88/NF-κB and ROS/AMPK pathway. Life Sci 291:120064.

McGeer PL, Itagaki S, Boyes BE, McGeer EG (1988) Reactive microglia are positive for HLA-DR in the substantia nigra of Parkinson's and Alzheimer's disease brains. Neurology 38: 1285-1291.

McMillan KJ, Murray TK, Bengoa-Vergniory N, Cordero-Llana O, Cooper J, Buckley A, Wade-Martins R, Uney JB, O'Neill MJ, Wong LF, Caldwell MA (2017) Loss of microRNA-7 regulation leads to alpha-synuclein accumulation and dopaminergic neuronal loss in vivo. Mol Ther 25:2404-2414.

Meng XH, Sun B, Xue MY, Xu P, Hu FH, Xiao ZD (2016) Comparative analysis of microRNA expression in human mesenchymal stem cells from umbilical cord and cord blood. Genomics 107:124-131.

Niu JL, Jin ZQ, Hyunbae Kim ZQ, Kolattukudy PE (2015) MCP-1-induced protein attenuates post-infarct cardiac remodeling and dysfunction through mitigating NF-κB activation and suppressing inflammation-associated microRNA expression. Basic Res Cardiol 110: 26.

Ouchi Y, Yoshikawa E, Sekine Y, Futatsubashi M, Kanno T, Ogusu T, Torizuka T (2005) Microglial activation and dopamine terminal loss in early Parkinson's disease. Ann Neurol 57:168-175.

Pan BT, Johnstone RM (1983) Fate of the transferrin receptor during maturation of sheep reticulocytes in vitro: selective externalization of the receptor. Cell 33: 967-978.

Patel DC, Tewari BP, Chaunsali L, Sontheimer H (2019) Neuron-glia interactions in the pathophysiology of epilepsy. Nat Rev Neurosci 20:282-297.

Paxinos G, Watson C (2006) The rat brain in stereotaxic coordinates. San Diego: Academic Press.

Perets N, Betzer O, Shapira R, Brenstein S, Angel A, Sadan T (2019) Golden exosomes selectively target brain pathologies in neurodegenerative and neurodevelopmental disorders. Nano Lett 19: 3422-3431.

Qu M, Lin Q, Huang L, Fu Y, Wang L, He S, Fu Y, Yang S, Zhang Z, Zhang L, Sun X (2018) Dopamine-loaded blood exosomes targeted to brain for better treatment of Parkinson's disease. J Control Release 287:156-166.

Ransohoff RM, Cardona AE (2010) The myeloid cells of the central nervous system parenchyma. Nature 468:253-262.

Rehmsmeier M, Steffen P, Hochsmann M, Giegerich R (2004) Fast and effective prediction of microRNA/target duplexes. RNA 10:1507-1517.

Rivkin M, Simerzin A, Zorde-Khvalevsky E, Chai C, Yuval JB, Rosenberg N, Harari-Steinfeld R, Schneider R, Amir G, Condiotti R, Heikenwalder M, Weber A, Schramm C, Wege H, Kluwe J, Galun E, Giladi H (2016) Inflammation-induced expression and secretion of microRNA 122 leads to reduced blood levels of kidney-derived erythropoietin and anemia. Gastroenterology 151:999-1010.

Santovito D, Egea V, Bidzhekov K, Natarelli L, Mourão A, Blanchet X, Wichapong K, Aslani M, Brunßen C, Horckmans M, Hristov M, Geerlof A, Lutgens E, Daemen MJAP, Hackeng T, Ries C, Chavakis T, Morawietz H, Naumann R, Hundelshausen PV, et al. (2020) Autophagy unleashes noncanonical microRNA functions. Autophagy 16:2294-2296.

Sarkar S, Malovic E, Harishchandra DS, Ghaisas S, Panicker N, Charli A, Palanisamy BN, Rokad D, Jin H, Anantharam V, Kanthasamy A, Kanthasamy AG (2017) Mitochondrial impairment in microglia amplifies NLRP3 inflammasome proinflammatory signaling in cell culture and animal models of Parkinson's disease. NPJ Parkinsons Dis 3:30.

Shi CS, Shenderov K, Huang NN, Kabat J, Abu-Asab M, Fitzgerald KA, Sher A, Kehrl JH (2012) Activation of autophagy by inflammatory signals limits IL-1beta production by targeting ubiquitinated inflammasomes for destruction. Nat Immunol 13:255-263.

Shi J, Gao W, Shao F (2017) Pyroptosis: gasdermin-mediated programmed necrotic cell death. Trends Biochem Sci 42:245-254.

Shiue SJ, Rau RH, Shiue HS, Hung YW, Li ZX, Yang KD, Cheng JK (2019) Mesenchymal stem cell exosomes as a cell-free therapy for nerve injury-induced pain in rats. Pain 160:210-223.

Singla DK, Johnson TA, Dargani ZT (2019) Exosome treatment enhances anti-inflammatory M2 macrophages and reduces inflammation-induced pyroptosis in doxorubicin-induced cardiomyopathy. Cells 8:1224. .

Stefanova N (2022) Microglia in Parkinson's disease. J Parkinsons Dis 12:S105-112.

Tang Q, Lu B, He J, Chen X, Fu Q, Han H, Luo C, Yin H, Qin Z, Lyu D, Zhang L, Zhou M, Yao (2022) Exosomes-loaded thermosensitive hydrogels for corneal epithelium and stroma regeneration. Biomaterials 280:121320.

Tentillier N, Etzerodt A, Olesen MN, Rizalar FS, Jacobsen J, Bender D, Moestrup SK, Romero-Ramos M (2016) Anti-inflammatory modulation of microglia via CD163-targeted glucocorticoids protects dopaminergic neurons in the 6-OHDA Parkinson's disease model. J Neurosci 36:9375-9390.

Valadi H, Ekström K, Bossios A, Sjöstrand M, Lee JJ, Lötvall JO (2007) Exosome-mediated transfer of mRNAs and microRNAs is a novel mechanism of genetic exchange between cells. Nat Cell Biol 9:654-659.

Vilaça-Faria H, Salgado AJ, Teixeira FG (2019) Mesenchymal stem cells-derived exosomes: a new possible therapeutic strategy for Parkinson's disease? Cells 8:118.

Wang B, Huang X, Pan X, Zhang T, Hou C, Su WJ, Liu LL, Li JM, Wang YX (2020) Minocycline prevents the depressive-like behavior through inhibiting the release of HMGB1 from microglia and neurons. Brain Behav Immun 88:132-143.

Weiss ML, Medicetty S, Bledsoe AR, Rachakatla RS, Choi M, Merchav S, Luo YQ, Rao MS, Velagaleti G, Troyer D (2006) Human umbilical cord matrix stem cells: preliminary characterization and effect of transplantation in a rodent model of Parkinson's disease. Stem Cells 24:781-792.

Wiklander OP, Nordin JZ, O'Loughlin A, Gustafsson Y, Corso G, Mäger I (2015) Extracellular vesicle in vivo biodistribution is determined by cell source, route of administration and targeting. J Extracell Vesicles 4:26316.

Witwer KW, Soekmadji C, Hill AF, Wauben MH, Buzás EI, Vizio DD (2017) Updating the MISEV minimal requirements for extracellular vesicle studies: building bridges to reproducibility. J Extracell Vesicles 6:1396823.

Wu J, Kuang L, Chen C, Yang J, Zeng WN, Li T, Chen H, Huang S, Fu Z, Li J, Liu R, Ni Z, Chen L, Yang L (2019) miR-100-5p-abundant exosomes derived from infrapatellar fat pad MSCs protect articular cartilage and ameliorate gait abnormalities via inhibition of mTOR in osteoarthritis. Biomaterials 206:87-100.

Xia C, Zeng Z, Fang B, Tao M, Gu C, Zheng L, Wang Y, Shi Y, Fang C, Mei S, Chen Q, Zhao J, Lin X, Fan S, Jin Y, Chen P (2019) Mesenchymal stem cell-derived exosomes ameliorate intervertebral disc degeneration via anti-oxidant and anti-inflammatory effects. Free Radic Biol 143:1-15.

Xiong Y, Mahmood A, Chopp M (2017) Emerging potential of exosomes for treatment of traumatic brain injury. Neural Regen Res 12:19-22.

Yan B, Zhang Y, Liang C, Liu B, Ding FZ, Wang YL, Zhu B, Zhao RZ, Yu XY, Li YX (2020) Stem cell-derived exosomes prevent pyroptosis and repair ischemic muscle injury through a novel exosome/circHIPK3/FOXO3a pathway. Theranostics 10:6728-6742.

Yao R, Chen Y, Hao H, Guo Z, Cheng X, Ma Y, Ji Q, Yang X, Wang Y, Li X, Wang Z (2020) Pathogenic effects of inhibition of mTORC1/STAT3 axis facilitates Staphylococcus aureus-induced pyroptosis in human macrophages. Cell Commun Signal 18:187.

Yu D, Li YX, Wang MY, Gu JM, Xu WR, Cai H, Fang XJ, Zhang X (2022) Exosomes as a new frontier of cancer liquid biopsy. Mol Cancer 21:56.

Yu H, Liu X, Chen B, Vickstrom CR, Friedman V, Kelly TJ, Bai X, Zhao L, Hillard CJ, Liu QS (2021) The neuroprotective effects of the CB2 agonist GW842166x in the 6-OHDA mouse model of Parkinson's disease. Cells 10:3548.

Zhang B, Wang M, Gong A, Zhang X, Wu XD, Zhu YH, Shi H, Wu LJ, Zhu W, Qian H, Xu WR (2015) HucMSC-exosome mediated-Wnt4 signaling is required for cutaneous wound healing. Stem Cells 33:2158-2168.

Zhang FS, Guo JS, Zhang ZH, Qian YP, Wang G, Duan MQ, Zhao HY, Yang Z, Jiang XF (2022) Mesenchymal stem cell-derived exosome: a tumor regulator and carrier for targeted tumor therapy. Cancer Lett 526:29-40.

Zhang J, Zhang J, Zhang Y, Liu W, Ni W, Huang X, Yuan J, Zhao B, Xiao H, Xue F (2020) Mesenchymal stem cells-derived exosomes ameliorate intervertebral disc degeneration through inhibiting pyroptosis. J Cell Mol Med 24:11742-11754.

Zhang LY, Jin QQ, Hölscher C, Li L (2021) Glucagon-like peptide-1/glucose-dependent insulinotropic polypeptide dual receptor agonist DA-CH5 is superior to exendin-4 in protecting neurons in the 6-hydroxydopamine rat Parkinson model. Neural Regen Res 16:1660-1670.

Zhang SQ, Jiang LR, Hu HZ, Wang H, Wang XY, Jiang JH, Ma YY, Yang J, Hou Y, Xie DH, Zhang Q (2020) Pretreatment of exosomes derived from hUCMSCs with TNF-α ameliorates acute liver failure by inhibiting the activation of NLRP3 in macrophage. Life Sci 246:117401.

Zhang W, Wang Y, Kong YC (2019) Exosomes derived from mesenchymal stem cells modulate miR-126 to ameliorate hyperglycemia-induced retinal inflammation via targeting HMGB1. Invest Ophthalmol Vis Sci 60:294-303.

Zhang X, Zhang YM, Li R, Zhu LP, Fu BQ, Yan TH (2020) Salidroside ameliorates Parkinson's disease by inhibiting NLRP3-dependent pyroptosis. Aging (Albany NY) 12:9405-9426.

C-Editor: Zhao M; S-Editor: Li CH; L-Editor: Song LP; T-Editor: Jia Y